IEEE Access
Multidisciplinary | Rapid Review | Open Access Journal

Received June 27, 2020, accepted June 30, 2020, date of publication July 3, 2020, date of current version July 16, 2020.

Digital Object Identifier 10.1109/ACCESS.2020.3006888

A Traveling-Wave Linear Ultrasonic Motor Driven by Two Torsional Vibrations: Design, Fabrication, and Performance Evaluation

JIANYE NIU[1], JIANG WU[1], MIAOYAN CAO[2], AND LIJUN WU[2]
[1]State Key Laboratory of Reliability and Intelligence of Electrical Equipment, Hebei University of Technology, Tianjin 300130, China
[2]School of Mechanical Engineering, Yanshan University, Qinhuangdao 066004, China

Corresponding authors: Jiang Wu (wujiang@sonic.pi.titech.ac.jp) and Miaoyan Cao (jacmy@ysu.edu.cn)

This work was supported in part by the Science and Technology (S&T) Program of Hebei under Grant E2020103001, and in part by the China Postdoctoral Science Foundation under Grant 2019M660964.

ABSTRACT In this study, we design and fabricate a tank-track-shaped stator working in two torsional modes to form a traveling-wave (TW) linear ultrasonic motor (USM). The stator comprises two torsional transducers and two kidney-shaped vibrating bodies. When voltages with a certain phase are applied to the transducers, two in-phase TWs are excited on the vibrating bodies to frictionally drive the slider. Here, the torsional vibration guarantees strong electromechanical coupling, and meanwhile, the tank-track shape ensures plural driving points and low weight; these features may facilitate realizing high thrust force density and high power density of linear motors. To examine the feasibility, first, we constructed a stator prototype 116 mm in length, 91 mm in width, and 32 mm in thickness and explored its vibration properties. The minimal standing wave (SW) ratio reaches 1.21 and the small SW components are desirable for TW motors. Then, we measured the load characteristics and found that, at the working frequency of 54.34 kHz and the phase shift of $-110°$, the maximal thrust force and maximal output power were 96.1 N and 27.8 W, respectively. Moreover, the thrust force density and power density reached respectively 234.1 N/kg and 67.8 W/kg, relatively high compared to the values of most conventional linear motors. This study verifies the feasibility of our proposal and paves a new way of designing powerful linear USMs.

INDEX TERMS Linear ultrasonic motor, torsional vibration, traveling wave, thrust force density, power density.

I. INTRODUCTION

Ultrasonic motors (USMs) convert electrical energy to mechanical energy on the basis of inverse piezoelectric effect and achieve actuation by frictional force [1]–[3]. Different from electromagnetic motors, they possess the merits of quick response, self-locking at the power-off state, and absence of electromagnetic radiation [4]–[6]. In particular, linear USMs are potentially applicable to some electromechanical system (e.g., precision instruments and optical devices) [6]–[9] as some of them have satisfactorily large outputs (e.g., the maximal thrust force is $\sim$50 N and the maximal output power is $>$20 W) [10]–[13]. However, their thrust force densities and/or power densities are generally not high enough; this probably deteriorates the controllability of electromechanical system [14], [15]. Thus, it is necessary to enhance thrust force densities and power densities of linear USMs.

It is known that vibration modes have fundamental effect on thrust force density and power density [16], [17]. To date, linear motors mainly operate in bending/bending (B^2), longitudinal/longitudinal (L^2), and bending/longitudinal (B/L) modes [6]–[13], [18]–[21]. First, B^2 modes have been heavily exploited in conventional USMs. For instance, Liu *et al.* [2] excited two orthogonal bending vibrations on the stator's bilateral ends to form a standing-wave (SW) motor. Kondo *et al.* [22] bonded two groups of lead-zirconate-titanate (PZT) elements onto two ends of a rectangular bar and generated a traveling wave (TW) on the middle part to drive the slider. In general, lightweight is achievable with B^2 motors [1], [10], [23], [24], but their mechanical outputs are limited as electromechanical

The associate editor coordinating the review of this manuscript and approving it for publication was Giambattista Gruosso.

coupling of bending vibration is not strong [25], [26]. Second, several motors utilize L^2 modes as longitudinal vibration generally exhibits high electromechanical coupling [1], [3]. For example, Ting *et al.* [8] arranged two Langevin-type transducers in orthogonal directions and used the elliptical motions on connecting points of two transducers to achieve actuation; this method, however, limits the number of driving feet, resulting in low mechanical outputs [12]. Third, some motors are achieved by combining B/L vibrations [5], [9], [22]. Taking Yun *et al.*'s motor [9] as a typical example, its thrust force density reaches 202 N/kg, relatively high among linear motors with satisfactory performance. However, since its transducer should be sufficiently long to generate large driving force, the thrust force density and/or power density are seemingly difficult to increase through minimization.

In this study, we employ two torsional vibrations to form a TW linear motor. Here, two kidney-shaped vibrating bodies are connected onto bilateral surfaces of two parallelly-arranged torsional transducers to form a tank-track-shaped stator. Since the torsional transducers work in the 2nd modes, the bilateral surfaces oscillate in phase [26]. As a consequence, two TWs are excited on the vibrating bodies to drive the slider. Here, torsional/torsional (T^2) modes are chosen for the following reasons: First, electromechanical coupling is stronger for torsional vibration than for bending vibration [27], [28]; this may enhance the-stator-induced driving force [1], [10]. Second, since two TWs in phase exist on the vibrating bodies, whose lengths are smaller than one wavelength, it can be equivalently regarded that this motor has two driving feet [1], [14], [22]; this also contributes to enhancing driving force. Third, the stator's tank-track-shaped framework seemingly facilitates realizing lightweight. On the other hand, linear motors with T^2 modes have been rarely been reported up to now. Thus, it would be meaningful to test whether using T^2 modes can increase thrust force densities and power densities of linear motors.

In this paper, first, we designed and fabricated a T^2 stator to form a TW linear motor and systematically explored its vibration properties. Then, we investigated the load characteristics and made comparison with several conventional linear USMs.

II. DESIGN OF T^2 MOTOR

A. OVERALL STRUCTURE

As Fig. 1 depicts, the tank-track-shaped stator consists of two cylindrical transducers and two kidney-shaped vibrating bodies. To achieve lightweight, the transducers and vibrating bodies are made of duralumin (A7075) for its low density [29]. Besides, four groups of torsional PZT disks are arranged at the transducers' nodes to efficiently generate the 2nd torsional vibration, causing the bilateral surfaces to oscillate in phase. The used PZT is P51, produced by Yuke Corporation (Baoding, China) and its elastic, piezoelectric,

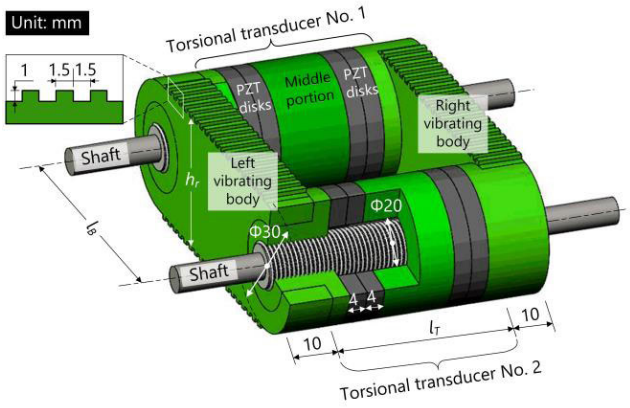

FIGURE 1. Configuration of the T^2 stator.

and dielectric matric are as follows:

$$\left[c^E\right] = \begin{bmatrix} 78 & 42 & 20 & 0 & 0 & 0 \\ 42 & 78 & 20 & 0 & 0 & 0 \\ 20 & 20 & 72 & 0 & 0 & 0 \\ 0 & 0 & 0 & 26 & 0 & 0 \\ 0 & 0 & 0 & 0 & 23 & 0 \\ 0 & 0 & 0 & 0 & 0 & 23 \end{bmatrix} \text{(GPa)},$$

$$[d] = \begin{bmatrix} 0 & 0 & 0 & 0 & 0.70 & 0 \\ 0 & 0 & 0 & 0.70 & 0 & 0 \\ -0.19 & -0.19 & 0.45 & 0 & 0 & 0 \end{bmatrix} \times 10^{-9}\text{(C/N)},$$

and

$$\left[\varepsilon^S\right] = \begin{bmatrix} 22.13 & 0 & 0 \\ 0 & 22.13 & 0 \\ 0 & 0 & 15.93 \end{bmatrix} \times 10^{-9}\ \text{(F/m)},$$

respectively. Note that, in the elastic matrix, c_{11}, c_{33}, and c_{55} are provided by the maker, and the other parameters are derived as $c_{44} = c_{33}/2/(1+\sigma)$, $c_{12} = c_{11} - 2c_{55}$, and c_{13} $(c_{23}) = c_{33} - 2c_{44}$, where σ stands for the Poisson's ratio [30]. The PZT disks and middle portions are tightly clamped with threaded parts of the stainless-steel shafts. Each vibrating body includes two semi-circular portions and a rectangular portion. Here, the semi-circular portions' diameters equal those of the transducers. The procedures of deciding the dimensions are introduced later. In addition, holes are created to insert the transducers into vibrating bodies. The procedures of assembling the stator is given in Appendix. A slider with a rectangular framework is pressed onto the stator and two poly-phenylene-sulfide sheets are glued onto the slider's bottom surface as frictional materials.

Fig. 2 illustrates the PZT disks' polarization directions and the method of applying voltage. The PZT disks are polarized along circumferential directions and each group contains two disks with opposite polarization directions. Phosphor-bronze electrodes are clamped onto the PZT disks' lateral surfaces for applying voltage. When two voltages with a certain phase shift are applied, as shown in Fig. 3, two torsional vibrations

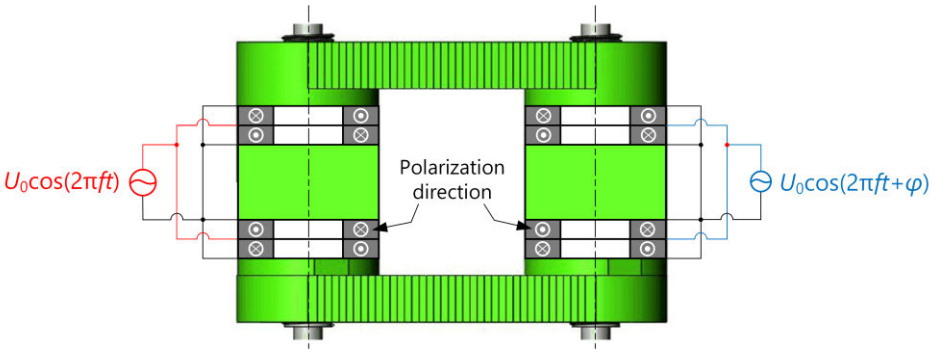

FIGURE 2. Polarization directions of PZT disks and the method of applying voltage.

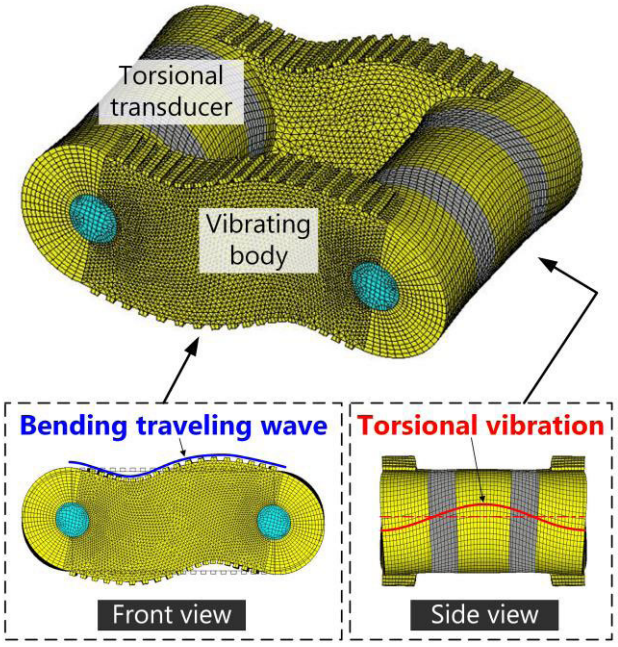

FIGURE 3. Conceptual view of the T^2 motor's working principle. Here, the mesh size is set to 1.5 mm.

are excited on the transducers and transferred into TWs on the vibrating bodies. As a result, elliptical motions exist on the upper surfaces and frictionally drive the slider.

B. DESIGN PROCEDURE

To obtain high thrust force density and high power density, we investigate how the k_{eff}/m ratio changes with varying dimension (where k_{eff} and m are respectively the effective electromechanical coupling factor and the stator's weight). Here, we focus on k_{eff} as it markedly affects USMs' mechanical outputs [2], [31], [32]. Besides, the resonance frequency f should be in the inaudible range (>20 kHz) to avoid the existence of noise.

(1) Set the PZT disk's diameter d_p and thickness to respectively 30 and 4 mm (see Fig. 1) as torsional PZT in this size is easy to produce [28].

(2) Make the torsional transducer's diameter d_T equal to d_p. For the 2nd torsional vibration,

$$f = \frac{1}{l_T} \cdot \sqrt{\frac{E}{2\,(1+\sigma)\,\rho}}, \tag{1}$$

where l_T denotes the transducer's length, and E, σ, and ρ represent the shear modulus (70.7 GPa), Poisson's ratio (0.33), and density (2.8×10^3 kg/m^3) of A7075, respectively.

(3) Determine the rectangular portion's length l_r. To excite TWs,

$$l_r = \frac{1+2n}{4} \cdot \lambda_B, \tag{2}$$

where n stands for an integer and λ_B denotes the wavelength corresponding to the bending vibration [1]. When $l_r = \lambda_B/4$, the distance between two torsional transducers' axes is likely smaller than d_T; this easily causes insufficient space for the transducers. On the other hand, considering the requirement of low weight, we set that [27], [33]

$$l_r = \frac{3}{4}\lambda_B = 1.01 \cdot \left(\frac{h_r}{f}\right)^{\frac{1}{2}} \cdot \left(\frac{E}{\rho}\right)^{\frac{1}{4}}, \tag{3}$$

where $h_r(= d_T)$ stands for the rectangular portion's height. Besides, the vibrating bodies have thicknesses of 10 mm, sufficiently high to obtain steady connection.

(4) Calculate k_{eff} through finite element analysis, of which the detailed procedures are given in [4] and [31]. In the meantime, m is derived by accumulating each part's weight.

Figs. 4(a) and (b) respectively show how k_{eff}/m ratios and fs depend on l_Ts. Clearly, the k_{eff}/m ratio reaches the peak value at $l_T = 40$ mm. Meanwhile, f equals ~50 kHz, locating in the inaudible range. According to Eq. 3, $l_r = 60.7$ mm.

(5) Create 1-mm-deep 1.5-mm-wide teeth (see Fig. 1) on upper and bottom surfaces of vibrating bodies to enlarge vibration amplitude. Here, the number of teeth is 19 for each surface.

Fig. 5 shows the stator prototype (weight: 0.41 kg). The stator is supported with shafts. Since the torsional vibration velocities are theoretically zero in torsional transducers' axes [16], this support method should exhibit negligibly small effect on the vibration properties [14].

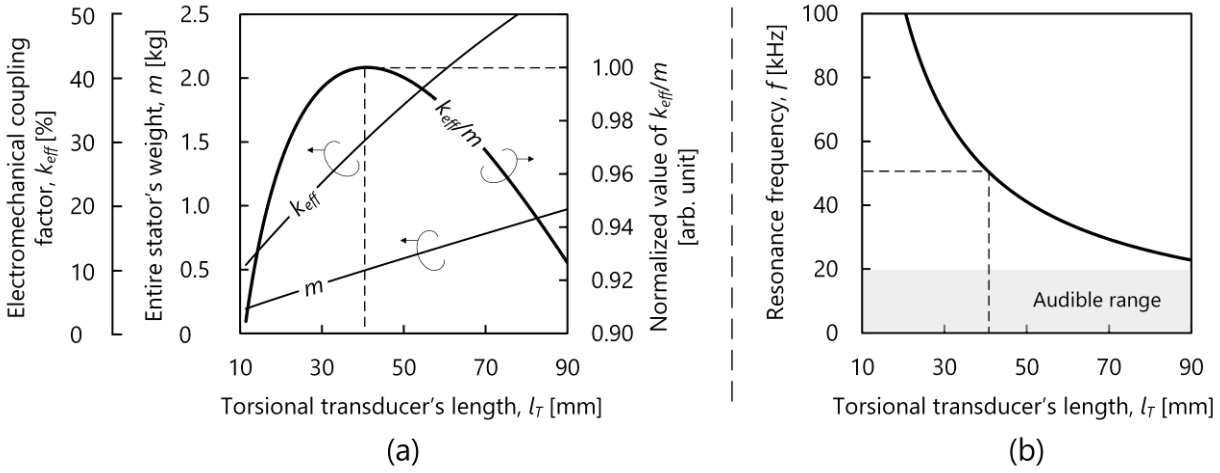

FIGURE 4. (a) Electromechanical coupling factors, entire stator's weight, and their ratio as well as (b) the resonance frequency versus torsional transducer's length.

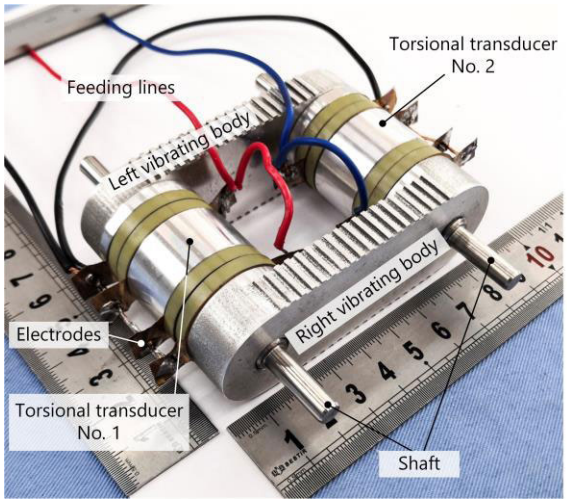

FIGURE 5. Photo of the stator.

III. VIBRATION PROPERTIES

First, the equivalent circuit parameters of the stator were explored with an impedance analyzer (4294A, Agilent, Santa Clara, USA). The resonance frequency f_r, anti-resonance frequency f_a, motional admittance Y_{m0}, and bandwidth corresponding to 0.707 times of peak admittance Δf were obtained from the admittance curves (note that they were measured when the transducers connected the vibrating bodies). Using these values, k_{eff}, mechanical quality factor Q_m, motional resistance R_m, motional capacitance C_m, and motional inductance L_m were estimated as [4], [14], [34]

$$k_{eff} = \sqrt{\frac{f_a^2 - f_r^2}{f_a^2}}, \tag{4}$$

$$Q_m = \frac{f_r}{\Delta f}, \tag{5}$$

$$R_m = \frac{1}{Y_{m0}}, \tag{6}$$

$$C_m = \frac{Y_{m0}}{2\pi f_r Q_m}, \tag{7}$$

and

$$L_m = \frac{Q_m}{2\pi f_r Y_{m0}}, \tag{8}$$

respectively. Table 1 lists the equivalent circuit parameters. Observably, f_rs have a discrepancy of <0.4 kHz between two torsional transducers; this facilitates the excitation of TWs. Besides, the calculated value of k_{eff} is ~30% (see Section II), in good agreement with the experimental results.

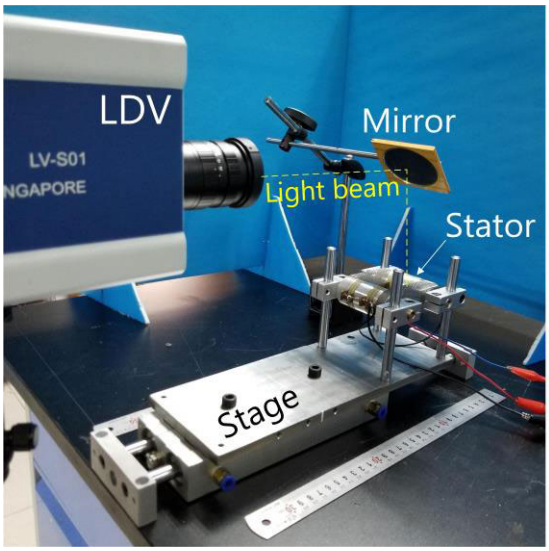

FIGURE 6. Experimental setup for measuring vibration velocity distribution.

Subsequently, the vibration velocity distribution was investigated via interferometric measurement [35]. The voltages were applied with power amplifiers (HSA4051, NF Corporation, Yokohama, Japan). As shown in Fig. 6, the stator was supported onto a frame and the z-axis vibration velocities on the upper surfaces of the vibrating bodies were measured with a laser Doppler vibrometer (LV-S01, Sunny Optical Technology Corp., Yuyao, China). The phase

TABLE 1. Equivalent circuit parameters.

Parameters	Transducer No. 1	Transducer No. 2
Resonance frequency f_r [kHz]	54.482	54.868
Anti-resonance frequency f_a [kHz]	57.098	57.878
Electromechanical coupling factor k_{eff}	30.4%	31.8%
Mechanical quality factor Q_m	195	182
Motional admittance Y_{m0} [mS]	10.2	11.0
Motional resistance R_m [Ω]	97.8	90.7
Motional capacitance C_m [nF]	0.153	0.176
Motional inductance L_m [mH]	55.8	47.8

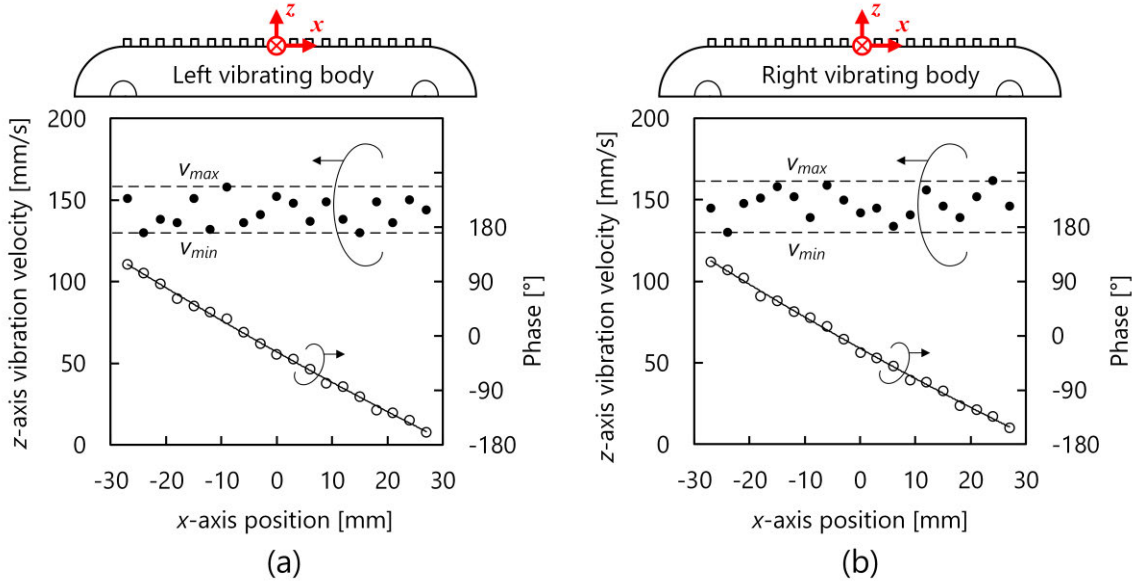

FIGURE 7. Vibration velocity distributions on (a) left and (b) right vibrating bodies.

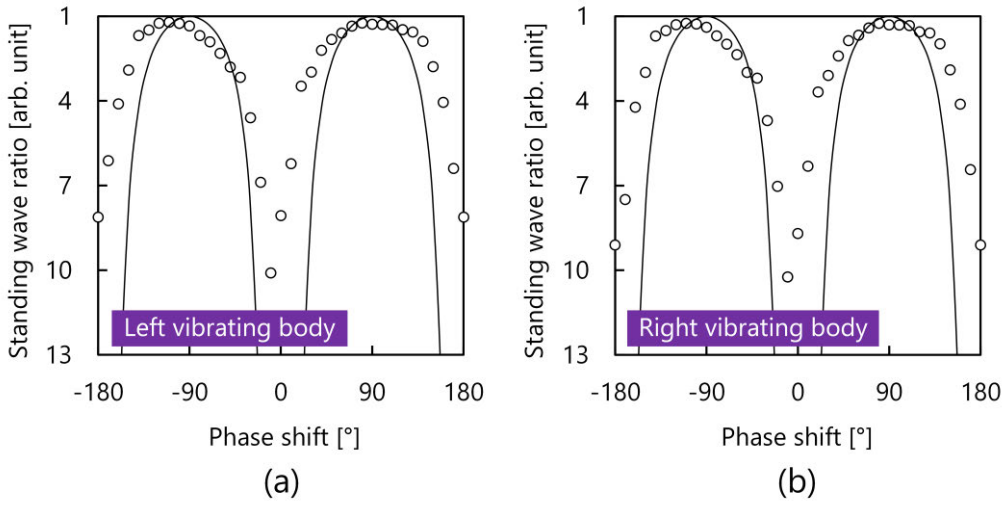

FIGURE 8. Standing wave ratios on (a) left and (b) right vibrating bodies. The circles and curves are simulated and measured results, respectively.

difference between the vibration velocity and a reference signal was obtained with an oscilloscope (MSO2000B, Tektronix, Oregon, USA). The driving voltage, working frequency, and phase shift were respectively set to 20 V, 54.34 kHz, and −110°. In this paper, the voltage and the vibration velocity are given as zero-to-peak values.

Figs. 7(a) and (b) respectively show how the z-axis vibration velocities are distributed on left and right vibrating

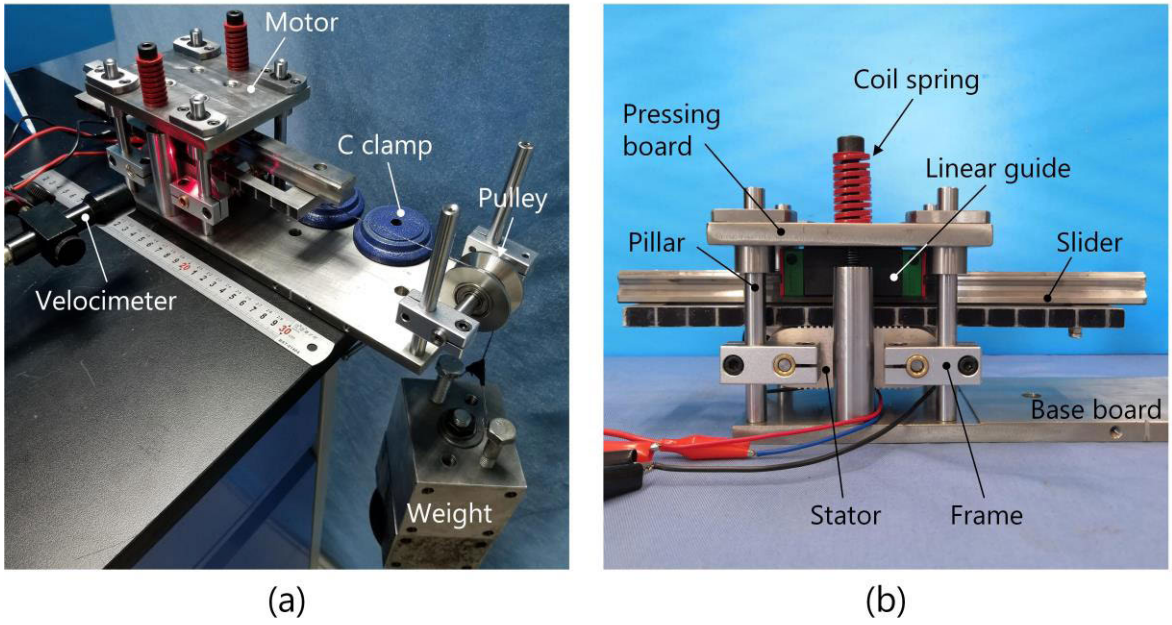

FIGURE 9. Testbed for evaluating load characteristics of the T^2 motor.

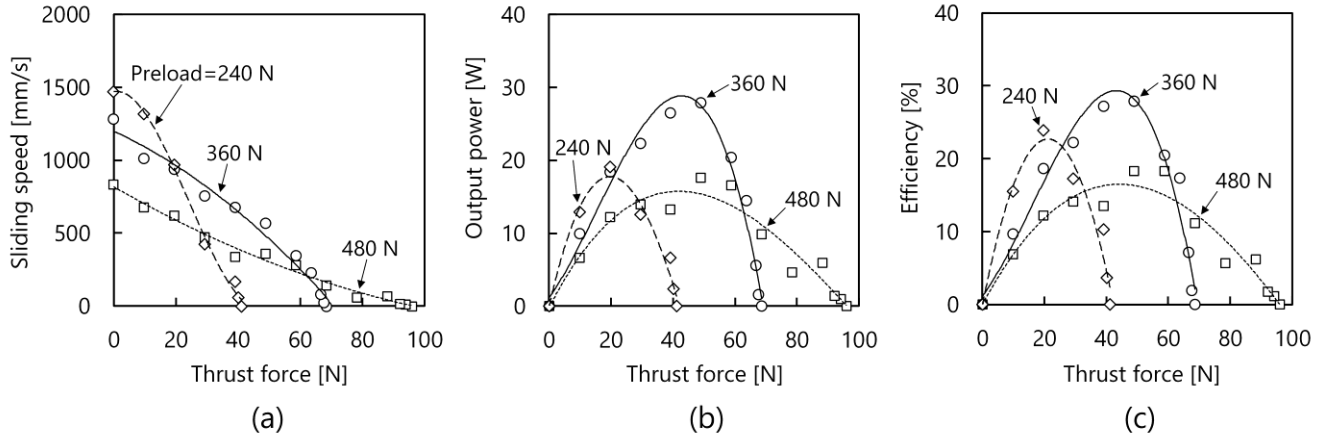

FIGURE 10. Load characteristics at 250 V. (a) Sliding speed, (b) output power, and (c) efficiency versus thrust force.

bodies. The phase difference gradually decreases from 120° to −150°, implying the successful excitation of TWs [34]. On the left vibrating body, the average vibration velocity is 143 mm/s, close to the value of the right vibrating body (144 mm/s); this can suppress frictional loss [1], [14], [36], [37]. Besides, the SW ratios (defined as v_{max}/v_{min} ratios, where v_{max} and v_{min} respectively denote maximal and minimal vibration velocities [38]) on the left and right vibrating bodies are 1.21 and 1.24, respectively, inferring that the SW components are satisfactorily small.

Finally, the relationship between the SW ratios and the phase shifts were explored. On condition that two SWs have a phase difference of $3\pi/2$ (corresponding to $3\lambda_B/4$) in space and a phase shift φ in the time domain, through superposition, the waves propagating on the vibrating bodies are expressed as [39]

$$\begin{aligned} &A_0 \cos(2\pi ft) \cos\left(\frac{2\pi}{\lambda_B} \cdot x\right) \\ &\quad + A_0 \cos(2\pi ft + \varphi) \cos\left(\frac{2\pi}{\lambda_B} \cdot x + \frac{3\pi}{2}\right) \\ &= A_0 \cos\left(2\pi ft + \frac{2\pi}{\lambda_B} \cdot x\right) \\ &\quad + A_0 \sin\left(\frac{2\pi}{\lambda_B} \cdot x\right) [\sin(2\pi ft) - \cos(2\pi ft + \varphi)], \end{aligned} \tag{9}$$

where A_0 stands for vibration amplitude. At $\omega t = 0$, magnitudes of the TW and SW components should be $|A_0|$

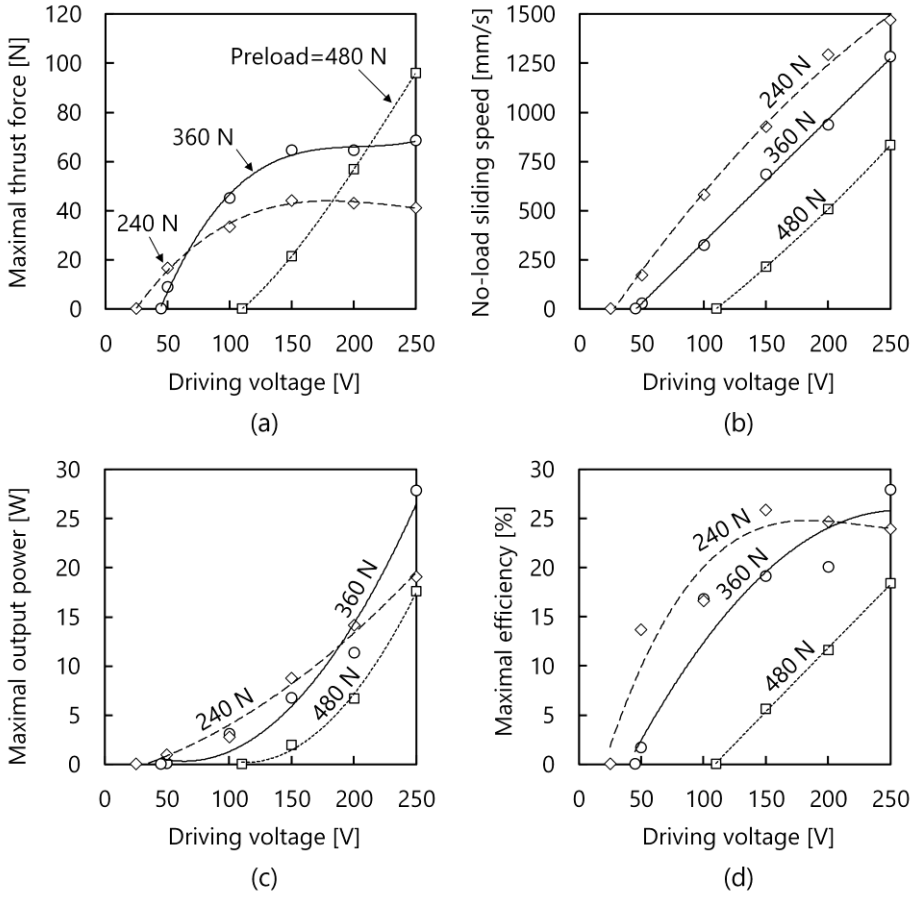

FIGURE 11. (a) Maximal thrust force, (b) no-load sliding speed, (c) maximal output power, and (d) maximal efficiency as functions of driving voltage.

and $|A_0\cos(\varphi)|$, respectively. Thus,

$$SW\ ratio = \frac{1 + |\cos(\varphi)|}{1 - |\cos(\varphi)|}. \tag{10}$$

Figs. 8(a) and (b) respectively plot the variations of SW ratios on the left and right vibrating bodies against the phase shift. Observably, the theoretical and experimental results show approximately the same tendencies. Since the two torsional transducers' admittance characteristics are not completely identical, their vibration amplitudes show small difference, which is a probable reason for the discrepancy between theoretical and experimental results [39]. In addition, the TW ratios provide minimum values when the phase shifts are $-110°$ and $80°$.

IV. MOTOR PERFORMANCE

A. LOAD CHARACTERISTICS

Fig. 9(a) illustrates the testbed for evaluating the T^2 motor's load characteristics. The thrust force was estimated by pulling up weights and the sliding speed was measured with a velocimeter (HG200, Aero-top Hi-tech Corp., Beijing, China). The input power was recorded using high-frequency power meters (3333, Hioki E. E. Corp., Nagano, Japan). Fig. 9(b) shows the entire motor's configuration. As mentioned above, the stator was supported with the frame that connected the pillars. One side of a linear guide was fixed to the slider while the other side was pressed with a board, capable of freely sliding along the pillars. Moreover, two coil springs were compressed to apply the preload to the motor. Here, the preload was estimated from the spring-stiffness coefficient and the spring's deformation. During the experiments, the working frequency and the phase shift were respectively set to ∼54.34 kHz and $-110°$.

Figs. 10(a), (b), and (c) show how the sliding speed, output power, and efficiency depend on the thrust force, respectively, at 250 V. When a 240 N preload was applied, the no-load sliding speed was 1470 mm/s and the maximal thrust force was 41.2 N. When the preload increased to 480 N, the maximal thrust force reached 96.1 N. At a 360 N preload, the maximal output power and the maximal efficiency were respectively 27.8 W and 27.9%.

Figs. 11(a), (b), (c), and (d) respectively show maximal thrust force, no-load sliding speed, maximal output power, and maximal efficiency as functions of the driving voltage. Initially, a dead region existed at <25 V. Subsequently, the thrust force became higher and saturated at a certain

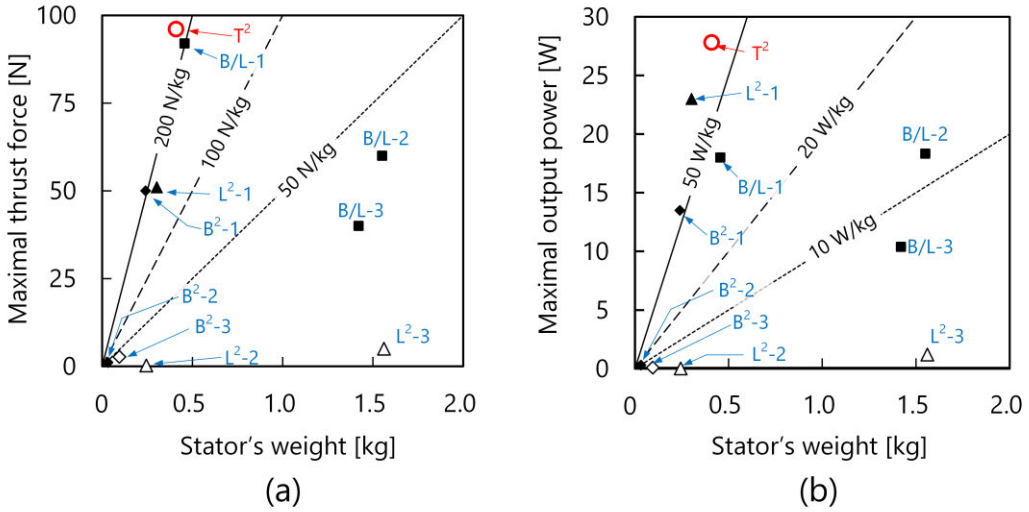

FIGURE 12. (a) Maximal thrust force and (b) maximal output power as functions of the stator's weight. Here, B-1, −2, and −3 represent the B^2 motors reported in [2], [7], and [8], respectively; L^2-1, −2, and −3 denote those reported in [9], [10], and [1], respectively; B/L-1, −2, and −3 are those reported in [11], [12], and [13] respectively; and T2 stands for the motor with two torsional modes. The empty and solid marks mean that the motors are driven with TWs and SWs, respectively.

TABLE 2. Performance comparison between the T^2 motor and typical ones.

No.	T^2	B^2-2	L^2-1	B/L-1
Reference	This motor	[7]	[8]	[9]
Stator's shape	Tank track	Non-uniform beam	V-shaped	Cylindrical
Stator's dimension [mm]	116×91×32	82×13.5×13.5	86×86×20	92×Φ40
Stator's weight [kg]	0.41	0.032	0.30	0.46
Number of driving feet	2	1	1	2
Working frequency [kHz]	54.34	31.05	~31	23.70
Maximal thrust force [N]	96	1.1	51	92
No-load sliding speed [mm/s]	1470	735	3500	470
Maximal output power [W]	27.8	0.3	23	18
Maximal efficiency	27.9%	–	28%	22%
Thrust force density [N/kg]	234	34.4	170	202
Power density [W/kg]	68	9.4	76	39

voltage. When the voltage ranged from 25 to 250 V, the no-load sliding speed exhibited a gradual enhancement. The output power and efficiency corresponding to 360 N were higher than those to 240 and 480 N probably because the frictional loss was smaller [40], [41]. Most TW motors cannot provide high efficiencies as the vibration velocities differ among the driving feet [21], [31], [35]. In contrast, only one wave crest exists on each vibrating body; this may suppress vibration-velocity-difference-induced frictional loss and consequently enhance the efficiency.

B. PERFORMANCE COMPARISON

Figs. 12(a) and (b) respectively plot the maximal thrust forces and maximal output powers of some linear motors against their stators' weights. The T^2 motor exhibits the thrust force density and power density of respectively 234.1 N/kg and 67.8 W/kg, relatively high compared to the values of most conventional ones. By comparing vibration properties and load characteristics of some typical motors, we get several possible reasons for high thrust force density and high power density of the T^2 motor.

(1) For the B^2-2 and T^2 motors, the PZT elements respectively work in the transverse (d_{31}) and shear (d_{15}) modes [7]. Consequently, the B^2-2 motor's k_{eff} (8.4%) is 0.27 times that of the T^2 motor (30.4%); this limits the thrust force density and power density of the B^2-2 motor [17].

(2) Though the L^2-1 motor's k_{eff} (26.6%) is comparable to that of the T^2 one, it has one driving foot [9], which probably results in the relatively low thrust force [12].

(3) Despite the small profile, the B/L-1 motor (in cylindrical shape) has larger weight, resulting in lower thrust force density and lower power density than the T^2 motor (in tank-track shape) [11]. It is also worth mentioning that, owing to identical configurations, two torsional transducers of the T^2 motor have approximately the same fs, ensuring

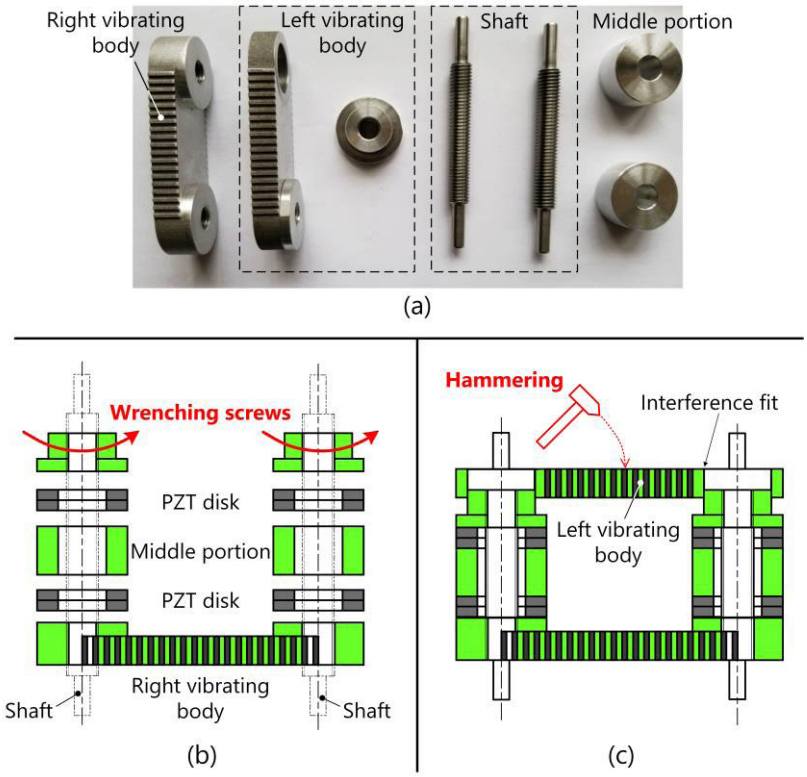

FIGURE 13. Assembly of the stator. (a) Photo of the components, (b) assembling the torsional transducers by wrenching screws, and (c) hammering the left vibrating body to form the entire stator.

its structural adaption to various application areas [1], [21]; this would be another advantage of the T^2 motor over the B/L one.

To sum up, high thrust force density and high power density are achievable with linear motors by using T^2 modes; this verifies the feasibility of our proposal. Besides, the production cost of the T^2 motor prototype is ∼300 dollars, twice the cost of the B^2, L^2, or B/L one as a consequence of relatively high expense of torsional PZT; this problem may be tackled in mass production owing to the reduction in PZT's expense.

V. CONCLUSION

In this study, we designed and fabricated a stator working in T^2 modes and employed it to form a linear motor. The stator incorporated two torsional transducers and two kidney-shaped vibrating bodies. When two voltages with a certain phase shift were applied, two torsional vibrations, excited on the transducers, generated two TWs on the vibrating bodies to frictionally drive the slider. To increase torque density and/or power density, electromechanical coupling factors and weights are discussed by FEA. The load characteristics of the T^2 motor are experimentally evaluated. The maximal thrust force, no-load sliding speed, maximal output power, and maximal efficiency are 96.1 N, 1470 mm/s, 27.8 W, and 27.9%, respectively. Moreover, since the torsional vibration, plural driving feet, and tank-track shape can enhance mechanical outputs and reduce weights, the thrust force density and power density reach respectively 234.1 N/kg and 67.8 W/kg, relatively high among conventional linear USMs.

Through the above investigation, we have gained an understanding on the T^2 motor and anticipate that the results will provide adequate information for structural optimization. In the future, the characteristics of the T^2 motor's stepping operation will be explored to achieve wider application fields.

APPENDIX

ASSEMBLY OF THE STATOR

The method of forming the tank-track-shaped stator is as follows:

(1) Machine the components, which, as Fig. 13(a) shows, include the kidney-shaped vibrating bodies, shafts, and middle portions. Here, the right vibrating body is structurally different from the left one.

(2) Clamp the middle portions, PZT disks, and parts of the left vibrating body onto the right vibrating body to form torsional transducers [see Fig. 13(b)].

(3) Insert the transducers into the left vibrating bodies' holes by hammering the vibrating body [see Fig. 13(c)]. Here, the outer surfaces of the connecting parts of the transducers

and the holes adopt interference fit for not only achieving steady connection but also avoiding excessive vibration loss [42], [43].

REFERENCES

[1] S. Ueha, Y. Tomikawa, M. Kurosawa, and K. Nakamura, *Ultrasonic Motors: Theory and Applications*. New York, USA: Oxford Univ. Press, 1993, pp. 4–13.

[2] Y. Liu, W. Chen, J. Liu, and X. Yang, "A high-power linear ultrasonic motor using bending vibration transducer," *IEEE Trans. Ind. Electron.*, vol. 60, no. 11, pp. 5160–5166, Nov. 2013.

[3] Q. Zhang, W. Chen, Y. Liu, J. Liu, and Q. Jiang, "A frog-shaped linear piezoelectric actuator using first-order longitudinal vibration mode," *IEEE Trans. Ind. Electron.*, vol. 64, no. 3, pp. 2188–2195, Mar. 2017.

[4] J. Wu, Y. Mizuno, and K. Nakamura, "Polymer-based ultrasonic motors utilizing high-order vibration modes," *IEEE/ASME Trans. Mechatronics*, vol. 23, no. 2, pp. 788–799, Apr. 2018.

[5] L. Wang, V. Hofmann, F. Bai, J. Jin, and J. Twiefel, "Modeling of coupled longitudinal and bending vibrations in a sandwich type piezoelectric transducer utilizing the transfer matrix method," *Mech. Syst. Signal Process.*, vol. 108, pp. 216–237, Aug. 2018.

[6] L. Wang, Y. Guan, Y. Liu, J. Deng, and J. Liu, "A compact cantilever type ultrasonic motor with nanometer resolution: Design and performance evaluation," *IEEE Trans. Ind. Electron.*, early access, Jan. 15, 2020, doi: 10.1109/TIE.2020.2965481.

[7] J. Yan, Y. Liu, J. Liu, D. Xu, and W. Chen, "The design and experiment of a novel ultrasonic motor based on the combination of bending modes," *Ultrasonics*, vol. 71, pp. 205–210, Sep. 2016.

[8] Y. Ting, C.-C. Li, L.-C. Chen, and C.-M. Yang, "Traveling-wave piezoelectric linear motor. II. Experiment and performance evaluation," *IEEE Trans. Ultrason., Ferroelectr., Freq. Control*, vol. 54, no. 4, pp. 854–860, Apr. 2007.

[9] M. Kuribayashi Kurosawa, O. Kodaira, Y. Tsuchitoi, and T. Higuchi, "Transducer for high speed and large thrust ultrasonic linear motor using two sandwich-type vibrators," *IEEE Trans. Ultrason., Ferroelectr., Freq. Control*, vol. 45, no. 5, pp. 1188–1195, Sep. 1998.

[10] L. Wang, T. Wielert, J. Twiefel, J. Jin, and J. Wallaschek, "A rod type linear ultrasonic motor utilizing longitudinal traveling waves: Proof of concept," *Smart Mater. Struct.*, vol. 26, no. 8, Aug. 2017, Art. no. 085013.

[11] C.-H. Yun, T. Ishii, K. Nakamura, S. Ueha, and K. Akashi, "A high power ultrasonic linear motor using a longitudinal and bending hybrid bolt-clamped Langevin type transducer," *Jpn. J. Appl. Phys.*, vol. 40, pp. 3773–3776, May 2001.

[12] Y. Liu, W. Chen, J. Liu, and S. Shi, "A rectangle-type linear ultrasonic motor using longitudinal vibration transducers with four driving feet," *IEEE Trans. Ultrason., Ferroelectr., Freq. Control*, vol. 60, no. 4, pp. 777–785, Apr. 2013.

[13] Y. Liu, J. Liu, W. Chen, and S. Shi, "A u-shaped linear ultrasonic motor using longitudinal vibration transducers with double feet," *IEEE Trans. Ultrason., Ferroelectr., Freq. Control*, vol. 59, no. 5, pp. 981–989, May 2012.

[14] K. Nakamura, *Ultrasonic Transducers: Materials and Design for Sensors, Actuators and Medical Applications*. Cambridge, U.K.: Woodhead Publishing Limited, 2012, pp. 677–704.

[15] D. Cook, *Robot Building for Beginners*, 2nd ed. New York, NY, USA: Springer-Verlag, 2009, pp. 236–239.

[16] K. Nakamura, M. Kurosawa, and S. Ueha, "Design of a hybrid transducer type ultrasonic motor," *IEEE Trans. Ultrason., Ferroelectr., Freq. Control*, vol. 40, no. 4, pp. 395–401, Jul. 1993.

[17] J. Wu, Y. Mizuno, and K. Nakamura, "Piezoelectric motor utilizing an alumina/PZT transducer," *IEEE Trans. Ind. Electron.*, vol. 67, no. 8, pp. 6762–6772, Aug. 2020.

[18] Y. Liu, J. Deng, and Q. Su, "Review on multi-degree-of-freedom piezoelectric motion stage," *IEEE Access*, vol. 6, pp. 59986–60004, 2018.

[19] W. Qiu, Y. Mizuno, D. Koyama, and K. Nakamura, "Efficiency improvement of hybrid transducer-type ultrasonic motor using lubricant," *IEEE Trans. Ultrason., Ferroelectr., Freq. Control*, vol. 60, no. 4, pp. 786–794, Apr. 2013.

[20] X. Li, Z. Yao, Y. Mi, X. Lin, C. Liang, and D. Wu, "Modeling, analysis and suppression of current harmonics of Langevin-type ultrasonic motors under high voltage," *Precis. Eng.*, vol. 64, pp. 177–187, Jul. 2020.

[21] D. Xu, Y. Liu, J. Liu, and W. Chen, "A bonded type ultrasonic motor using the bending of a crossbeam," *IEEE Access*, vol. 4, pp. 1109–1116, 2016.

[22] S. Kondo, H. Yamaura, D. Koyama, and K. Nakamura, "Traveling wave type ultrasonic linear motor using twin bending bars," *Phys. Procedia*, vol. 3, no. 1, pp. 1053–1058, Jan. 2010.

[23] Y. Liu, J. Yan, L. Wang, and W. Chen, "A two-DOF ultrasonic motor using a longitudinal–bending hybrid sandwich transducer," *IEEE Trans. Ind. Electron.*, vol. 66, no. 4, pp. 3041–3050, Apr. 2019.

[24] J. Wu, Y. Mizuno, M. Tabaru, and K. Nakamura, "Ultrasonic motors with polymer-based vibrators," *IEEE Trans. Ultrason., Ferroelectr., Freq. Control*, vol. 62, no. 12, pp. 2169–2178, Dec. 2015.

[25] M. Slabki, J. Wu, M. Weber, P. Breckner, D. Isaia, K. Nakamura, and J. Koruza, "Anisotropy of the high-power piezoelectric properties of $Pb(Zr,Ti)O_3$," *J. Am. Ceram. Soc.*, vol. 102, no. 10, pp. 6008–6017, Oct. 2019.

[26] Y. Tanoue and T. Morita, "Opposing preloads type ultrasonic linear motor with quadruped stator," *Sens. Actuators A, Phys.*, vol. 301, Jan. 2020, Art. no. 111764.

[27] K. F. Graff, *Wave Motion in Elastic Solids*. New York, NY, USA: Dover, 1991, pp. 204–209.

[28] *Properties of Piezo Ceramics*. Accessed: Jun. 20, 2020. [Online]. Available: http://www.fujicera.com/product/

[29] D. Tabor, *The Hardness of Metals*. New York, NY, USA: Oxford Univ. Press, 1951, pp. 2–4.

[30] T. Morita, *Piezoelectric Phenomena*, Tokyo, Japan: Morikita Publication, 2017, pp. 86–94.

[31] J. Wu, Y. Mizuno, and K. Nakamura, "Structural parameter study on polymer-based ultrasonic motor," *Smart Mater. Struct.*, vol. 26, no. 11, Nov. 2017, Art. no. 115022.

[32] D. Xu, Y. Liu, S. Shi, J. Liu, W. Chen, and L. Wang, "Development of a nonresonant piezoelectric motor with nanometer resolution driving ability," *IEEE/ASME Trans. Mechatronics*, vol. 23, no. 1, pp. 444–451, Feb. 2018.

[33] J. Wu, Y. Mizuno, M. Tabaru, and K. Nakamura, "Measurement of mechanical quality factors of polymers in flexural vibration for high-power ultrasonic application," *Ultrasonics*, vol. 69, pp. 74–82, Jul. 2016.

[34] H. Dong, Z. Yu, K. T. V. Grattan, T. Sun, and T. Li, "Acoustic standing wave field measurement using a laser Doppler vibrometer based on the Hankel Fourier algorithm," *IEEE Access*, vol. 7, pp. 139013–139020, Sep. 2019.

[35] J. Wu, Y. Mizuno, and K. Nakamura, "A traveling-wave ultrasonic motor utilizing a ring-shaped alumina/PZT vibrator," *Smart Mater. Struct.*, vol. 28, no. 12, Dec. 2019, Art. no. 125017.

[36] K. Nakamura, M. Kurosawa, and S. Ueha, "Characteristics of a hybrid transducer-type ultrasonic motor," *IEEE Trans. Ultrason., Ferroelectr., Freq. Control*, vol. 38, no. 3, pp. 188–193, May 1991.

[37] K. Nakamura and S. Ueha, "Potential ability of ultrasonic motors: A discussion focused on the friction control mechanism," *Electron. Commun. Jpn. (Part II, Electron.)*, vol. 81, no. 4, pp. 57–68, Apr. 1998.

[38] D. Kong and M. K. Kurosawa, "Stator optimization and evaluation method in a surface acoustic wave motor," *Jpn. J. Appl. Phys.*, vol. 54, Jul. 2015, Art. no. 07HB01.

[39] T. Ide, J. R. Friend, K. Nakamura, and S. Ueha, "A low-profile design for the noncontact ultrasonically levitated stage," *Jpn. J. Appl. Phys.*, vol. 44, no. 6B, pp. 4662–4665, Jun. 2005.

[40] T. Cao, X. Li, B. Wang, Y. Mi, G. Zhao, J. Twiefel, and D. Wu, "Viscoelastic analytical model and design of polymer-based bimodal piezoelectric motor," *Mech. Syst. Signal Process.*, vol. 145, Nov. 2020, Art. no. 106960.

[41] J. Wu, Y. Mizuno, and K. Nakamura, "A rotary ultrasonic motor operating in torsional/bending modes with high torque density and high power density," *IEEE Trans. Ind. Electron.*, early access, Jun. 10, 2020, doi: 10.1109/TIE.2020.3000112.

[42] K. Adachi, "High-power ultrasonic transducer—A designing method for bolt-clamped Langevin-type transducers and its application," (in Japanese), *J. Jpn. Soc. Prec. Eng.*, vol. 75, no. 4, pp. 479–483, Apr. 2009.

[43] K. Nakamura, "Evaluation methods for materials for power ultrasonic applications," *Jpn. J. Appl. Phys.*, vol. 59, Jun. 2020, Art. no. SK0801.

JIANYE NIU received the B.S. degree in mechanical engineering, and the M.S. and Ph.D. degrees in mechatronics engineering from Yanshan University, Qinhuangdao, China, in 2005, 2008, and 2019, respectively.

He is currently a Senior Engineer with the School of Mechanical Engineering, Hebei University of Technology, Tianjin, China. His research interests include parallel mechanism and its applications, rehabilitation robots, mechanical engineering, and artificial neural networks.

JIANG WU was born in Liaoning, China, in January 1988. He received the B.E. degree in mechanical engineering from the Dalian University of Technology, China, in 2010, the M.E. degree in mechatronics engineering from the State Key Laboratory of Robotics and Systems, Harbin Institute of Technology, China, in 2012, and the Dr.Eng. degree in electrical and electronics engineering from the Laboratory for Future Interdisciplinary Research of Science and Technology, Tokyo Institute of Technology, Japan, in 2017.

His research interests include piezoresistive and piezoelectric materials, permanent magnet-based sensing technology, and polymer-based ultrasonic transducers and actuators.

MIAOYAN CAO was born in Hunan, China, in January 1978. He received the B.S. degree in mechatronics engineering and the Ph.D. degree in mechanical design and theory from Yanshan University, Qinhuangdao, China, in 2001 and 2012, respectively.

His research interests include the ultrasonic assisted forming of tube/sheet metal and light alloy forming process.

LIJUN WU received the M.E. degree from Yanshan University, Qinhuangdao, China, in 2012, where he is currently pursuing the Ph.D. degree with the Laboratory of Advanced Forging and Stamping Technology and Science, School of Mechanical Engineering.

His current research interests include ultrasonic vibration assisted plastic process, electro-hydraulic servo and proportional control, and heavy machinery fluid power transmission and control.